RESEARCH ARTICLE

annalen der physik
www.ann-phys.org

Optomechanical Coupling Optimization in Engineered Nanocavities

*S. Edelstein, J. Gomis-Bresco, G. Arregui, P. Koval, N. D. Lanzillotti-Kimura, D. Torrent, C. M. Sotomayor-Torres, and P. D. García**

In optomechanics, the interaction between light and matter is enhanced by engineering cavities where the electromagnetic field and the mechanical displacement are confined simultaneously within the same volume. This leads to a wide range of interesting phenomena, such as optomechanically induced transparency and the cooling of macroscopic objects to their lowest possible motion state. In this manuscript, the focus is on designed optomechanical cavities exploiting heterostructures in air-slot photonic-crystal waveguides, incorporating different hole shapes and dimensions to engineer and control their optomechanical properties. The aim is to maximize the optical quality factor of the optical cavity, while ensuring optical mode volumes below the diffraction limit. These optimized optical modes interact with in-plane motional degrees of freedom of the structures achieving high optomechanical coupling rates, thus opening up the possibility of mechanical amplification, nonlinear dynamics and chaos through the optomechanical back-action.

1. Introduction

The interaction of light with the motional degrees of freedom of nanoscale objects may lead to decoherence as the electromagnetic energy can be inelastically scattered from and to the vibrations of the system.[1] However, when carefully confined within a high-quality optical resonator the interplay between the electromagnetic field and the motion of the resonator itself leads to a wide range of rich dynamics.[2] Cavity optomechanics exploits this regime in which the radiation pressure of photons exerts a substantial force on the mechanical oscillator, leading to mechanical motion that, in turn, modifies the optical field itself. This coupling mechanism has enabled groundbreaking experiments, ranging from the precise detection of minute displacements in mechanical oscillators[3] to the manipulation of individual quantum states.[4] The field of cavity-optomechanics has experienced unprecedented growth due to its ability to enable highly sensitive measurements,[5] novel-device functionalities,[6] and applications in quantum information processing[7] in nano and micrometer scaled systems.

The increasing need of miniature components in scalable platforms such as silicon[8] requires ever smaller systems for optical signal processing,[9] modulation,[10] as well as emerging quantum technologies.[11] An optomechanical resonator offers highly coherent and integrated mechanical elements with nonlinear dynamics such as chaos,[12] injection-locking,[13] or frequency combs[14] that are suitable to implement these functionalities in integrated circuits. The simultaneous confinement of mechanical and optical degrees of freedom in optomechanical and phononic resonators further increases the strength and speed of the interaction, allowing faster and more efficient energy transfer at lower powers.[15] Near-infrared optical photons and gigahertz phonons are excellent for this as they are coupled efficiently and matched to one another in micro and nanostructures, as both have wavelengths on the order of micrometers. Smaller optomechanical systems demand less energy to achieve the same effects but it becomes increasingly challenging to improve their degree of optical confinement and their photon–phonon coupling strength simultaneously.

A high optomechanical coupling strength enables the operation in the sideband-resolved regime where the sidebands induced on the optical cavity by the modulation due to the

S. Edelstein, P. D. García
Instituto de Ciencia de Materiales de Madrid (ICMM)
Consejo Superior de Investigaciones Científicas (CSIC)
Sor Juana Inés de la Cruz 3, Madrid 28049, Spain
E-mail: pd.garcia@csic.es

J. Gomis-Bresco, G. Arregui, C. M. Sotomayor-Torres
Catalan Institute of Nanoscience and Nanotechnology (ICN2)
CSIC and The Barcelona Institute of Science and Technology
Campus UAB, Bellaterra, Barcelona 08193, Spain

P. Koval
Simune Atomistics
Tolosa Hiribidea 76, Donostia 20018, Spain

N. D. Lanzillotti-Kimura
Université Paris-Saclay, CNRS
Centre de Nanosciences et de Nanotechnologies
Palaiseau 91120, France

D. Torrent
GROC, UJI
Institut de Noves Tecnologies de la Imatge (INIT)
Universitat Jaume I
Casteló de la Plana 12071, Spain

C. M. Sotomayor-Torres
ICREA - Institució Catalana de Recerca i Estudis Avançats
Barcelona 08010, Spain

The ORCID identification number(s) for the author(s) of this article can be found under https://doi.org/10.1002/andp.202300417

DOI: 10.1002/andp.202300417

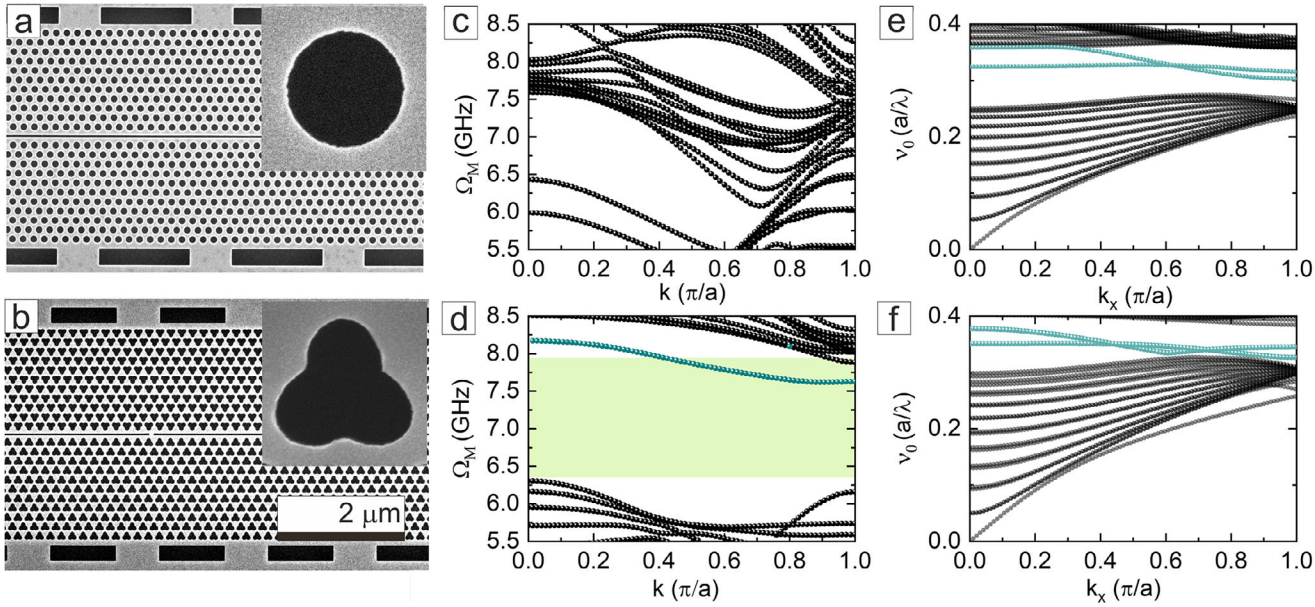

Figure 1. Engineered optomechanical cavities in slow-light and slow-sound waveguides. Scanning electron microscopy (SEM) micrograph of a photonic-crystal waveguide with an air slot fabricated in silicon with circular holes (a) (Ref. [16]) and shamrock holes (b) (Ref. [6]). The lattice periodicity in both waveguides is $a = 470$ nm, the air slot width $s = 55$ nm, and membrane thickness $t = 220$ nm. The circular hole radius $r = 140$ nm and the shamrocks are three slightly overlapping elliptical holes with semi-minor axis of 94 nm and semi-major axis of 126 nm. (c,d) are the phonon dispersion relation for circular-and shamrock-holes waveguides, respectively. (e,f) are the optical dispersion relation for circular-and shamrock-holes waveguides, respectively.

mechanical oscillation are spectrally well resolved from the optical mode itself.[2] In this regime, the mechanical frequency is usually significantly lower than the optical one, allowing for precise characterization and control of the confined electromagnetic mode through dynamical backaction.[2] The key figures of merit in this regime are the optomechanical coupling, g_{OM} (the strength of interaction between the mechanical oscillator and the optical field), the optical linewidth or quality factor, $Q = \nu/\Delta\nu$ (where ν is the optical resonant frequency and $\Delta\nu$ the optical linewidth), and the frequency of the mechanical motion, Ω_m. A high value of g_{OM} ensures efficient transfer of energy and information between the mechanical and optical domains and it determines the potential to manipulate and control the mechanical motion using light. The optical quality factor Q is determined by the spectral linewidth of the optical cavity and quantifies the energy dissipation and loss in the optical oscillator. A high optical Q-factor implies low damping and loss, resulting in longer coherence times enabling optomechanical operation at lower vibrational frequencies. Finally, the mechanical frequency Ω_m determines the spectral resolution of the sideband regime, its spectral working range, as it sets the spectral separation between the sidebands and the optical mode itself. Overall, operating at high values of g_{OM}, Q, and Ω_m is desirable to perform optomechanical amplification and cooling[2] ensuring precise characterization and manipulation of the system of interest.

In this manuscript, we explore two silicon-integrated nanophotonic systems based on a slow-light waveguiding mechanism to optimize the optomechanical sideband-resolved regime. We analyze two modified versions of a standard photonic-crystal waveguide, **Figure 1**a,b, with two different hole dimensions and shapes: circles[16] and shamrocks.[6,17] The shamrocks are formed by overlapping three elliptical holes as explained elsewhere.[17] In both systems, we include an air slot of width $s = 55$ nm etched along the waveguide axis[18–20] to confine the electromagnetic field in air with very large group index, $n_g = c/|v_g|$, at the Brillouin Zone edge. The group velocity $v_g = d\omega/dk$ is given by the slope of the fundamental waveguide mode which at $k = \pi/a$ is nearly flat (see Figure 1e,f). The air-slot photonic-crystal slab cavity has been widely studied with circular holes[18,21–24] while the shamrock-shape holes has been tested experimentally[6,16,17] only very recently to study disorder-induced cavity-optomechanics.[6,16] In absence of any confining mechanism, the vibrations in silicon slabs are delocalized within the whole structure with frequencies ranging from hundreds of MHz to few GHz as seen in the phonon dispersion relation plotted in Figure 1c. However, just by reshaping the hole from a circular to a shamrock, it is possible to open a full and wide frequency gap of destructive interference in the GHz range,[17] as plotted in Figure 1d. The mechanism behind this interference effect is the anisotropic re-distribution of the mass within the unit cell which creates masses connected by necks playing the role of strings inducing a strong constructive and destructive interference effect. Heterostructure cavities[25] combining both circular and shamrock holes have shown large optomechanical couplings between a single optical cavity and two distinct microwave-frequency mechanical modes.[26] Here, we follow a rigorous approach, varying two independent geometrical parameters, to optimize the photon–phonon coupling in heterostructre air-slot photonic-crystal cavities.

We create a cavity by reducing the length of a single unit of lattice with respect to the one of the waveguide (i.e., breaking the symmetry of the waveguide). We then adiabatically tune the horizontal pitch along the waveguide axis from a central defect unit cell ($a_c = 460$ nm) to mirror unit cells ($a = 470$ nm) on both sides. The full defect region is formed by $Nc = 15$ unit cells. Breaking

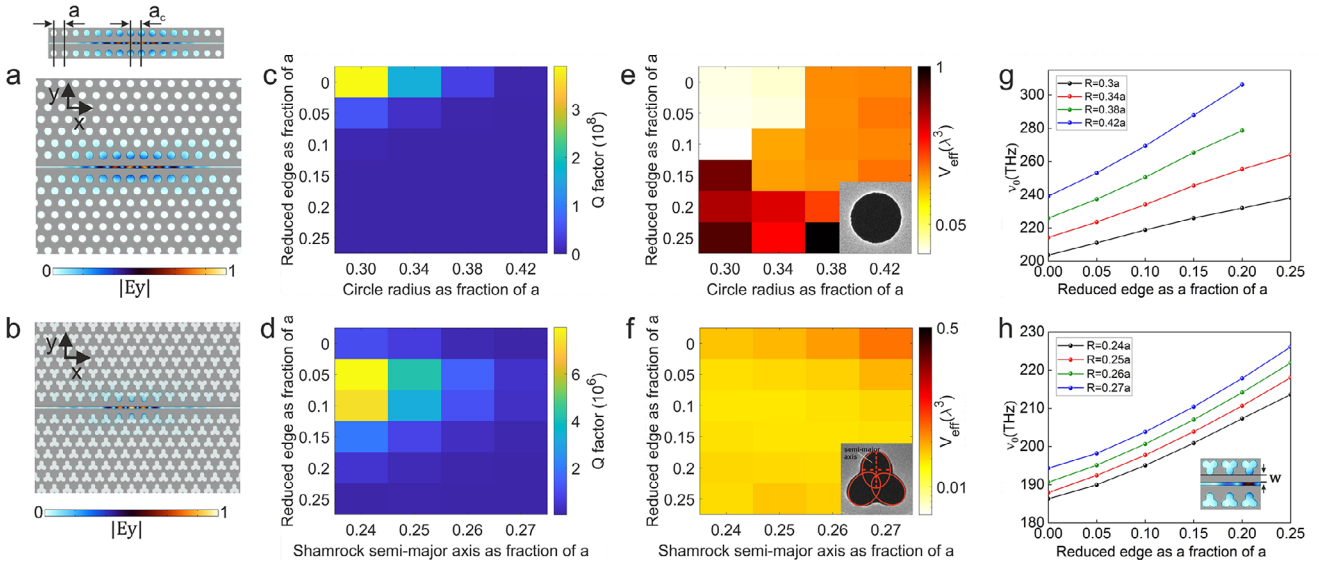

Figure 2. Optical cavity: Effect of hole size and slab edge width (near the air slot) on fundamental mode's Q factor, effective mode volume (V_{eff}) and resonant frequency in air slot optical cavities. a,b) Electromagnetic field component $|E_y|$ of fundamental mode of air slot photonic crystal cavities with circular and shamrocks holes, respectively. c,d) Q factor of fundamental mode of circular and shamrock holes cavities, respectively. e,f) Effective mode volume of fundamental mode in cavity with circular and shamrocks holes, respectively. g,h) Effect of reducing slab edge on the resonant frequency of the fundamental mode of cavities with circular and shamrocks holes respectively, for various values of hole size (R).

the symmetry of the waveguide creates a confinement potential for THz photons. The optical confinement is due to a spectral mismatch between the photonic gaps induced by lattice-constant difference between the two crystals. **Figure** 2a,b plots the electromagnetic field ($|E_y|$ component) of the fundamental cavity mode of photonic-crystal heterostructure cavity where holes have circular (a) and shamrock (b) shapes. It can be seen that the field is indeed confined in the central region where the defect is formed.

In our optimization analysis, we explore a parameter space formed by the hole size and the width of the slab edge near the air slot. Figure 2(c,d), depicts the Q factor of the cavity's fundamental mode for different values of hole size and reduced edge of slabs with circular and shamrock holes. Our calculations show that while slabs with circular holes are optimized without the need of a further reduction of the slab edge, slabs with shamrock holes reach higher quality factors when reducing the slab edge by $0.05a - 0.1a$. In both systems, smaller holes generate higher Q factors. To calculate the photonic eigenmodes and their dispersion relations, we used the guided-mode expansion method.[27] In order to calculate their Q factors, we used the finite-element method which gives more accurate results.[28] The implementation of the guided-mode expansion currently available[29] belongs to so-called fully-differentiable implementations that offers access to the computed properties and their gradients using methods of automatic differentiation. We have implemented a slightly modified version of the guided-mode expansion which is simpler and easier to extend as it is not aiming at differentiability of the results.

Besides the optical Q factor, another crucial property for any optical nanocavity is the level of spatial confinement of the light field, i.e. the effective mode volume, V_{eff}. Regardless of the precise application targeted for the cavity (Purcell enhancement, two-photon absorption, Kerr non-linearities, etc.), this figure-of-merit determines the strength of the light-matter interaction in combination with the intrinsic optical losses characterized by the Q factor. Here, we use the following definition for the effective mode volume:

$$V_{\text{eff}} = \frac{\int_V \varepsilon(\mathbf{r})|\mathbf{E}(\mathbf{r})|^2 \mathbf{dr}}{\varepsilon(\mathbf{r}_o)|\mathbf{E}(\mathbf{r}_o)|^2} \tag{1}$$

where $\mathbf{r}_o$ is the position of maximum electric field intensity. Figure 2(e,f) plot the effective mode volume of the cavity's fundamental mode varying the hole size and edge width. Since the electromagetic field is confined mostly within the air slot, the mode volumes of the cavities are all very small, mostly below $0.03(\lambda/n_{air})^3$. The resulting figure of merit for light-matter interaction, Q/V_{eff}, for the systems considered here is significantly high, $10^7 < Q/V_{\text{eff}} < 10^9$. This efficient light-matter interaction is promising not only for optomechanics but for nonlinear optics,[30] sensing,[31] or to enhance the interaction between optical excitations and free-electron beams.[32]

In the structures optimized here, the electromagnetic field is mostly confined within the subwavelength air slot, as shown in Figure 2(a,b), becoming extremely sensitive to variations of the slot size due to local vibrations. This translates into the modulation of the optical cavity at frequencies corresponding to the ones of the differential motion itself that allows precise sensing of mechanical displacement of the nanostructure.[18–20] To calculate the natural frequencies of the vibrations of our structures and their optomechanical coupling to the optical cavity modes, we use a finite-element method. The GHz phonon dispersion of the waveguides forming the heterostructure cavities are plotted in Figure 1c, d. Observing their phononic response, the advantage of using the shamrock-shape holes with respect to the simple

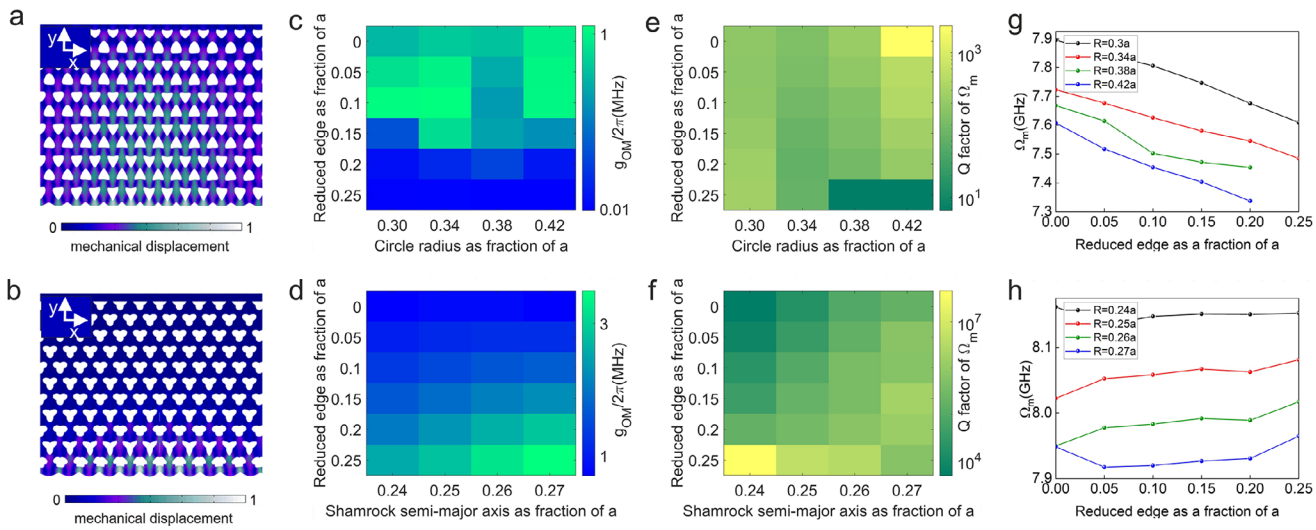

Figure 3. Optomechanical coupling rate in air-slotted heterostructure-optomechanical cavities. a,b) Displacement amplitude, $|\mathbf{Q}(r)|$, and deformation profiles of highest-coupling mechanical modes of heterostructure cavities with circular and shamrock holes, respectively. c,d) Optomechanical coupling rates ($g_{OM}/2\pi$) calculated between cavity's fundamental mode (see Figure 2a,b) and highest coupling mechanical modes Figure 3a,b for various values of hole size and edge width of heterostructure cavities with circular and shamrock holes, respectively. e,f) Q factor of highest coupling mechanical mode for various values of hole size and edge width of heterostructure cavities with circular and shamrock holes, respectively. g,h) Effect of reducing slab edge on the highest-coupling mechanical mode frequency (Ω_m) for various values of hole size (R), for circular and shamrock holes, respectively.

circular ones becomes clear. A lattice of circular holes enables the creation of a THz photonic bandgap but has very little impact on the vibrational modes of the nanostructure. As shown in Figure 1c, circular holes do not open a bandgap in the phononic dispersion relation and there are mechanical modes present in the whole 5–8 GHz range. The shamrock-shaped waveguide, on the contrary, has a strong impact on the hypersonic phonon transport in these systems as it opens a wide full gap for GHz vibrations in addition to the THz photonic gap, see Figure 1d. The shamrock holes slabs have no mechanical vibrations between 6.5 and 8.5 GHz apart from the guided mode. This allows creating a heterostructure cavity that confines simultaneously THz photons and GHz phonons **Figure** 3d.

To quantify the optomechanical coupling rate, we consider both the frequency shift due to the moving dielectric boundary and the photo-elastic effect, so that $g_{OM} = g_{OM,MB} + g_{OM,PE}$. Due to the confinement of the electromagnetic field within the air slot, the optomechanical coupling rate of the fundamental modes is mainly due to the moving dielectric boundary effect and the photo-elastic effect contributes less than 10% to coupling rate. The (lowest-order) optomechanical coupling rate in a deformable cavity is given by Ref. [33] is obtained as:

$$g_{\mathrm{OM,MB}} = X_{ZPF}\frac{\nu_0}{2}\frac{\int (\mathbf{Q}(\mathbf{r})\cdot\hat{n})(\Delta\epsilon|\mathbf{E}^{\parallel}|^2 - \Delta(\epsilon^{-1})|\mathbf{D}^{\perp}|^2)dA}{\int \epsilon(\mathbf{r})|\mathbf{E}(\mathbf{r})|^2 d^3\mathbf{r}} \quad (2)$$

where $\mathbf{Q}(\mathbf{r})$ is the mechanical displacement field, $\mathbf{E}^{\parallel}$ is the electric field parallel to the surface of integration and $\mathbf{D}^{\perp}$ is the electric displacement field perpendicular to this surface. $\Delta\epsilon = \epsilon_{slab} - \epsilon_{air}$, $\Delta(\epsilon^{-1}) = 1/\epsilon_{slab} - 1/\epsilon_{air}$, ν_0 is the optical angular frequency. This is a pure rate, and is found by multiplying the dispersion of the optical cavity resonance with mechanical oscillator displacement by the zero-point fluctuation amplitude of the mechanical oscillator. $X_{ZPF} = \sqrt{\frac{\bar{h}}{2m_{eff}\Omega_m}}$ where $m_{eff} = \int \rho|\mathbf{Q}(\mathbf{r})|^2 d^3\mathbf{r}$ is the effective mass of the mechanical mode, Ω_m is the mechanical angular frequency, ρ is the density of the slab material and $\bar{h}$ is the reduced Planck constant.

In Figure 3c,d, we plot the calculated optomechanical coupling rate between the optical cavities' fundamental modes (Figure 2a,b) and the highest coupling mechanical modes whose displacement amplitude and deformation profiles are depicted in Figure 3a,b for cavities with circular and shamrock holes, respectively. While the mode displacement of the cavity with circular holes is extended over the whole slab, the displacement of the shamrock holes' cavity is confined to the slab edge. The optomechanical coupling rates of the shamrock cavity are about three times higher than the circular holes cavity. Additionally, we plot in Figure 3e,f the Q factor of those high-coupling mechanical modes, calculated as $Q(\Omega_m) = \frac{\Omega_{m_r}}{2\Omega_{m_i}}$ where Ω_{m_r} is the real part of the eigenfrequency Ω_m, and Ω_{m_i} is its imaginary part. The mechanical quality factor is a measure of the energy decay rate in each cycle of vibrations. The higher the Q factor, the longer that coherent energy will remain in the mode prior to leaking into the environment. While the mechanical Q factors of the circular holes cavities are very low, the mechanical Q factors of the shamrock cavities reach values as high as 4×10^7 precisely due to the confining potential enabled by the shamrock shape. We used Finite element-method (FEM) for the simulation of the complete structures and to determine the mechanical mode frequency (Ω_m), the mechanical Q factors and the optomechanical coupling rate ($g_{OM}/2\pi$).

With our rigorous optimization method it is possible to create heterostructure cavities that confine both light and phonons over a large THz spectral range with optomechanical coupling rates $\simeq$ MHz range. The presence of a gap in the phonon

dispersion relation for shamrocks enables large coupling rates for optical cavities and spatially and spectrally isolated vibrations only in this case. These vibrations induce a local variation in the slot width, Δs, which modulates the resonance frequency of optical guided modes. Although it is possible to find these type of edge-vibrational modes also in the case of circular-shape holes, they only become simultaneously spatially and spectrally well confined in the shamrock-shape structure. This allows selective single- and multimode operation,[26] phonon routing,[17] and high degree of control over the characterization and manipulation of the system.

In summary, we have analyzed two different nanoscale systems with different geometries that simultaneously confine the electromagnetic field in the THz range and phonons in the GHz range, enabling their coupling efficiently. We explore two different approaches to obtain slow-light waveguides with an air slot where the confined electromagnetic field is becoming very sensitive to differential motion of the nanostructure. We follow a heterostructure cavity confinement strategy to modify the lattice period of the waveguide by creating a confinement potential. The geometry of the lattice and, in particular, the shape of the holes are crucial to engineer the frequency of the motional degrees of freedom. To optimize the performance of these photomechanical structures, we target as figures of merit of this regime the optical quality factor, Q, the frequency of the mechanical motion Ω_m, which determines the spectral operational frequency range, and the coupling rate g_{OM} between photonic and phononic resonances of the system. In the two systems studied here, we obtain values of $Q \simeq 10^6$ and vibrations with frequencies $\Omega_m \simeq 7 - 8\,\mathrm{GHz}$ and optomechanical coupling rates g_{OM} of kHz up to 3 MHz. While the more standard circular shapes do not lead to efficient spectral and spatial mechanical confinement, shamrock-shape lead to vibrations that are spatially and spectrally well isolated. This not only enables a large and efficient coupling to the optical cavities but also ensures a controllable operation of the resulting photomechanical cavity deep under the sideband-resolved regime. In addition, the optomechanical cavities analyzed here show excellent light-matter interaction figures of merit of up to $Q/V_{\mathrm{eff}} \simeq 10^9(\lambda^3)$. The air-confinement of the optical cavity modes make them suitable for ultrahigh sensitive and controlled optomechanical operation as well as photon–phonon interactions mediated by trapped atoms.[34]

Acknowledgements

This work was supported by the Spanish Minister of Science, Innovation and Universities via the Severo Ochoa Program (Grant no. SEV-2017-0706), as well as by the CERCA Program/Generalitat de Catalunya and the EU-H2020 FET Proactive project TOCHA (no. 824140). P.D.G. gratefully acknowledges the support by the national project PID2021-124814NB-C21 (SPHAM) and the HORIZON-EIC-2022 pathfinder project NEUROPIC (Grant no. 101098961). D.T. acknowledged the support by the HORIZON-EIC-2021 pathfinder project DYNAMO (Grant no. 101046489). C.M.S.T acknowledged the support of the national project SIP (Grant no. PGC2018-104333-BI00).

Conflict of Interest

The authors declare no conflict of interest.

Data Availability Statement

The data that support the findings of this study are available from the corresponding author upon reasonable request.

Keywords

cavity-optomechanics, nanostructures, phononics, silicon photonics

Received: September 18, 2023
Revised: March 2, 2024
Published online:

[1] L. Brillouin, *Ann. Phys.* **1922**, *9*, 88.
[2] M. Aspelmeyer, T. J. Kippenberg, F. Marquardt, *Rev. Mod. Phys.* **2014**, *86*, 1391.
[3] T. Liu, F. Pagliano, R. van Veldhoven, V. Pogoretskiy, Y. Jiao, A. Fiore, *Nat. Commun.* **2020**, *11*, 2407.
[4] M. J. Weaver, F. Buters, F. Luna, H. Eerkens, K. Heeck, S. de Man, D. Bouwmeester, *Nat Commun* **2017**, *8*, 824.
[5] B.-B. Li, L. Ou, Y. Lei, Y.-C. Liu, *Nanophotonics* **2021**, *10*, 2799.
[6] G. Madiot, R. C. Ng, G. Arregui, O. Florez, M. Albrechtsen, S. Stobbe, P. D. García, C. M. Sotomayor-Torres, *Phys. Rev. Lett.* **2023**, *130*, 106903.
[7] S. Barzanjeh, A. Xuereb, S. Gröblacher, M. Paternostro, C. A. Regal, E. M. Weig, *Nat. Phys.* **2022**, *18*, 15.
[8] W. Bogaerts, D. Pérez, J. Capmany, D. A. B. Miller, J. Poon, D. Englund, F. Morichetti, A. Melloni, *Nature* **2020**, *586*, 207.
[9] A. P. Ovvyan, M.-K. Li, H. Gehring, F. Beutel, S. Kumar, F. Hennrich, L. Wei, Y. Chen, F. Pyatkov, R. Krupke, W. H. P. Pernice, *Nat. Commun.* **2023**, *14*, 3933.
[10] Z. Yu, X. Sun, *ACS Photonics* **2021**, *8*, 798.
[11] J. Wang, F. Sciarrino, A. Laing, M. G. Thompson, *Nat. Photonics* **2020**, *14*, 273.
[12] D. Navarro-Urrios, N. E. Capuj, M. F. Colombano, P. D. García, M. Sledzinska, F. Alzina, A. Griol, A. Martínez, C. M. Sotomayor-Torres, *Nat. Commun.* **2017**, *8*, 14965.
[13] G. Arregui, M. F. Colombano, J. Maire, A. Pitanti, N. E. Capuj, A. Griol, A. Martínez, C. M. Sotomayor-Torres, D. Navarro-Urrios, *Nanophotonics* **2021**, *10*, 1319.
[14] P. E. Allain, B. Guha, C. Baker, D. Parrain, A. Lemaître, G. Leo, I. Favero, *Phys. Rev. Lett.* **2021**, *126*, 243901.
[15] A. H. Safavi-Naeini, D. V. Thourhout, R. Baets, R. V. Laer, *Optica* **2019**, *6*, 213.
[16] G. Arregui, R. C. Ng, M. Albrechtsen, S. Stobbe, C. M. Sotomayor-Torres, P. D. García, *Phys. Rev. Lett.* **2023**, *130*, 043802.
[17] O. Florez, G. Arregui, M. Albrechtsen, R. C. Ng, J. Gomis-Bresco, S. Stobbe, C. M. Sotomayor-Torres, P. D. García, *Nat. Nanotechnol.* **2022**, *17*, 947.
[18] A. H. Safavi-Naeini, T. P. M. Alegre, M. Winger, O. Painter, *Appl. Phys. Lett.* **2010**, *97*, 181106.
[19] X. Luan, Y. Huang, Y. Li, J. F. McMillan, J. Zheng, S.-W. Huang, P.-C. Hsieh, T. Gu, D. Wang, A. Hati, D. A. Howe, G. Wen, M. Yu, G. Lo, D.-L. Kwong, C. W. Wong, *Sci. Rep.* **2014**, *4*, 6842.
[20] M. Winger, T. D. Blasius, T. P. M. Alegre, A. H. Safavi-Naeini, S. Meenehan, J. Cohen, S. Stobbe, O. Painter, *Opt. Express* **2011**, *19*, 24905.
[21] Y. Li, J. Zheng, J. Gao, J. Shu, M. S. Aras, C. W. Wong, *Opt. Express* **2010**, *18*, 23844.
[22] M. Nomura, *Opt. Express* **2012**, *20*, 5204.
[23] W. Shimizu, N. Nagai, K. Kohno, K. Hirakawa, M. Nomura, *Opt. Express* **2013**, *21*, 21961.

[24] A. Pitanti, J. M. Fink, A. H. Safavi-Naeini, J. T. Hill, C. U. Lei, A. Tredicucci, O. Painter, *Opt. Express* **2015**, *23*, 3196.
[25] B.-S. Song, S. Noda, T. Asano, Y. Akahane, *Nat. Mater.* **2005**, *4*, 207.
[26] G. Madiot, M. Albrechtsen, S. Stobbe, C. M. Sotomayor-Torres, G. Arregui, *APL Photonics* **2023**, *8*, 116107.
[27] L. C. Andreani, D. Gerace, *Phys. Rev. B* **2006**, *73*, 235114.
[28] M. Minkov, V. Savona, *Sci. Rep.* **2014**, *4*, 5124.
[29] M. Minkov, I. A. D. Williamson, L. C. Andreani, D. Gerace, B. Lou, A. Y. Song, T. W. Hughes, S. Fan, *ACS Photonics* **2020**, *7*, 1729.
[30] C. Koos, P. Vorreau, T. Vallaitis, P. Dumon, W. Bogaerts, R. Baets, B. Esembeson, I. Biaggio, T. Michinobu, F. Diederich, W. Freude, J. Leuthold, *Nat. Photonics* **2009**, *3*, 216.
[31] J. Jágerská, H. Zhang, Z. Diao, N. L. Thomas, R. Houdré, *Opt. Lett.* **2010**, *35*, 2523.
[32] F. J. García de Abajo, V. Di Giulio, *ACS Photonics* **2021**, *8*, 945.
[33] A. H. Safavi-Naeini, O. Painter, *Opt. Express* **2010**, *18*, 14926.
[34] J.-B. Béguin, Z. Qin, X. Luan, H. J. Kimble, *Proc. Nat. Acad. Sci.* **2020**, *117*, 29422.